Design and Comparative Analysis of Ultra-wideband and High Directive Antennas for THz Applications

Ali Yahyaoui [1], Jawad Yousaf [2], Amira Dhiflaoui [3], Majid Nour [1], Mohamed Zarouan [1], Mohammed Aseeri [4], and Hatem Rmili [1]

[1] Electrical and Computer Engineering Department, Faculty of Engineering, King Abdulaziz University
P.O. Box 80204, Jeddah 21589, Saudi Arabia
hmrmili@kau.edu.sa

[2] Department of Electrical, Computer and Biomedical Engineering, Abu Dhabi University, United Arab Emirates

[3] University of Tunis El Manar (UTM), National Engineering School of Tunis (ENIT)
Communications Systems Laboratory (SysCom), BP 37, Belvédère 1002 Tunis, Tunisia

[4] National Center for Telecommunications and Defense System Technologies (TDST)
King Abdulaziz City of Science and Technology (KACST), Riyadh, Saudi Arabia

Abstract ─ This work presents a comprehensive detailed comparative study of the three ultra-wideband and high directive antennas for the THz imaging, spectroscopy, and communication applications. Three different types of photoconductive antennas (log-spiral, Vivaldi, and bowtie antennas) are designed and simulated in the frequency range of 1 to 6 THz in the CST microwave studio (MWS). The enhanced directivity of the designed PCAs is achieved with the integration of the hemispherical silicon-based lens with the PCA gold electrode and quartz substrate of the proposed antennas. The performance of the designed PCAs is compared in terms of impedance and axial ratio bandwidths, directivity, and radiation efficiency of the proposed antennas. The reported log spiral, Vivaldi PCAs with added silicon lens exhibit the -10 dB impedance bandwidth of 6 THz, 3dB AR bandwidth of 5 THz, 6 THz, and 6 THz and peak total radiation efficiencies of 45%, 65%, and 95% respectively.

Index Terms ─ Bowtie antenna, high directivity, log spiral antenna, photoconductive THz antenna, Vivaldi antenna, wideband.

I. INTRODUCTION

The development of the terahertz (THz) technology is helping to alleviate the crowded microwave band spectrum for the wide range of future applications in the field of high-speed (terabit-per-second) wireless communication system, spectroscopy, imaging, sensing, material characterization, and medical fields [1-7]. The 3 mm to 30 μm free-space wavelength (or 0.1 to 10 THz) band is referred to as the THz frequency band. This band is gaining a lot of attention because of the distinctive characteristics of the non-ionizing nature of THz radiations, easy penetration through various materials, and their minimal effect on the human body [4, 7-9].

The photoconductive antennas (PCAs) are among the favorite choices of the THz antenna designers for the generation of THz radiations due to their associated advantages of broadband radiations, compact size as well as normal operation at the room temperature [8, 10, 11]. In PCA, THz waves are generated with the interaction of the ultrafast femtosecond photon with the biased photoconductive substrates having ultra-short (sub-picosecond) carrier lifetime as well as ultrafast carrier mobility. The common examples of used substrates for this purpose are LTGaAs [10, 12, 13], SiGaAs [10, 14], and InGaAs [10, 15]. Besides the aforementioned advantages, the limitation of the PCA includes the low optical-to-THz conversion efficiency [4, 8] which limits its applications especially for the imaging systems which demands high directive and polarization-insensitive THz radiations.

The commonly employed approaches for the enhancement of the laser coupling to increase the conversion efficiency of the PCAs are 3D nonplasmonic structures [16], anti-reflection coatings of PCA substrates [17, 18], plasmonic nanoantennas [19] and electrodes [20]. The requirements of the electron beam lithography for the fabrication of the PCAs using proposed approaches [16-20] significantly increase the time and cost of the fabrication process [4]. The reported other examples of the photoconductive antennas are bow tie [8, 11, 17, 21], dipole planner array [22], Yagi-Uda [23], spiral-shaped [24], and the conical horn [25]. The researchers used the microlens array [12, 13, 17, 21, 26, 27], adding of the

Submitted On: July 8, 2020
Accepted On: December 31, 2020
https://doi.org/10.47037/2020.ACES.J.360311

1054-4887 © ACES

silicon-based lenses on the PCA structures [8, 17, 21, 25, 28], and sandwiching of an antenna structure with metasurfaces [8, 22] for the enhancement of the poor directivity performance of the designed THz antennas. Although the utilization of the aforementioned approaches results in the enhancement of the directivity of the realized antennas, the reported designs [8, 11, 17, 21-25, 28, 29] have limitations of lower impedance bandwidth (0.2 THz to 1 THz), axial ratio (AR) bandwidth, and overall large size of reported antenna designs.

In this work, we report a detailed comparative study about the design and analysis of the three different types of the ultra-wideband, high directive, and high-efficiency PCAs for the frequency range of the 1 to 6 THz. The realized antenna designs are of log spiral [6] (Fig. 1), Vivaldi [7] (Fig. 2), and bowtie [9] (Fig. 3) types. The full-wave EM simulation of the proposed THz antennas is performed in CST MWS for the frequency range of 1 to 6 THz without the lens. Subsequently, the directivity performance of the proposed antennas is enhanced by adding a silicon-based hemispherical lens on the backside of the used quartz ($\varepsilon_r = 3.78$, $\tan\delta = 0.0001$) substrate of the antennas. The study compares the performance of the reported antennas in terms of impedance bandwidth, axial ratio bandwidth, and radiation characteristics (gain, directivity, efficiency) of the antennas. The reported log spiral, Vivaldi, and bowtie PCAs exhibit the -10 dB impedance bandwidth of 6 THz respectively. The observed 3dB AR bandwidth is 5 THz, 6 THz, and 6 THz for the designed spiral, Vivaldi, and bowtie antenna structure with the lens. The peak values of the total radiation efficiencies for the realized spiral, Vivaldi, and bowtie antenna structure with the lens are 45%, 65%, and 95% respectively. The observed -10 dB impedance and 3-dB AR bandwidth of the designed optimized antenna with the lens are the largest among all the reported legacy designs [8, 11, 17, 21-25, 28, 29] as per our best knowledge.

The structure of the rest of the paper is as follows. Section II presents a comprehensive review of the performance of the legacy THz antennas. The details about the design of the reported three antennas are described in Section III. Section IV details the comparison of the performance of the reported antennas without the lens. The comparison of the designed antennas performance with the added lens in the antenna structure is presented in Section V. Last section VI concludes the study.

II. RELATED WORK

This section presents a comprehensive review of the relevant reported designs of the non-nano based PCA antenna designs. The authors in [23] reported a Yagi-Uda antenna without a lens with high input impedance in the frequency range of 580 GHz to 600 GHz. The design of a spiral-shaped THz antenna working in the frequency range of 1.8 – 2.05 THz is reported in [24]. In [11], Park *et al.* covered the antenna structure with metal nanoislands to form nanoplasmonic PCA for the increase in the emission properties of the antenna.

Jyothi *et al.* [21] reported a bow-tie PCA with a Si-hemispherical lens for the enhanced directivity in the frequency range of 1 to 1.2 THz. The authors in [17] investigated the effect of the dielectric coating and added hemispherical Si-lens on bow-tie PCA structure for the enhancement of optical-to-THz conversion efficiency of the designed antenna. The authors in [28] proposed that the utilization of the aspheric lenses can improve the radiation coupling of the PCAs. Deva *et al.* [25] reported a fixed-frequency (0.8 THz) conical horn and Si-lens based PCA for the gain enhancement with the better physical fitting of the horn-shape with commercially available Si-lenses.

In [8, 29], authors combined the PCA with the artificial magnetic conductor (AMC) [8] and metasurface-based flat lens [29] for the enhancement of directivity of the antenna without the need of large-sized silicon-based lenses as needed for [17, 21, 25]. In [22], authors combined the planner dipole array with frequency selective surface to enhance the radiation properties of the array type PCA. However, the integration of the metasurface in the antenna structure increases the side-lobe levels and front-to-back ratio of the antenna. Array design of antennas are used to enhance the radiation efficiency and front to back ratio of the antennas at the cost of the large antenna size [8, 23, 24, 30]. Generally, the periodic structures are used for the enhancement of the antenna bandwidth. However, as reported in [31], the use of a log-periodic circular-toothed structure with an outer diameter of 1.28 mm results in relatively lower bandwidth (< 1 THz). It depicts that the proper designing of the periodic antenna structure is essential to achieve the wideband operation.

Table 1 summarizes the performance of the reviewed designs in terms of the antenna type, used substrate, the material of antenna electrodes, lens, impedance bandwidth, AR bandwidth, and directivity. The maximum impedance bandwidth of 1 THz for the non-lens based THz antenna is reported for the nano THz antenna of [11]. The integration of the lens enhances the directivity to 18.5 dBi for [25] with maximum noted bandwidth of 0.80 THz for the dipole array PCA of [28]. As shown in Table 1, the reported -10 dB impedance bandwidths for the PCA structures with frequency selective surfaces (FSS) are 0.18 THz [8] and 0.37 THz [22], respectively.

The proposed log-spiral, Vivaldi, and bowtie PCAs did not only produce the high directivity but also exhibit wideband impedance and AR bandwidths characteristics as compared to all reviewed legacy designs of [8, 11, 17, 21-25, 28, 29].

Table 1: Comparison of proposed UWB PCA design with the legacy design

References	Antenna Type	Substrate	Antenna Electrode Material	Lens/FSS	-10 dB Impedance Bandwidth (THz)	Maximum Directivity (dBi)
Han [23]	Yagi-Uda	GaAs	Ti-Au	No lens	0.02	10.9
Singh et al. [24]	Spiral-shaped	Si	Al	No lens	0.25	-
Park [11]	Nanoplasmonic bow-tie PCA	GaAs	Cr/Au	No lens	1.00	-
Jyothi [21]	Bow-tie PCA	GaAs	TiAu /AuGe / AuCr	Si hemispherical lens	0.20	10.85
Gupta et al. [17]	Bow-tie PCA with a dielectric coating	SI-GaAs	AuGe	HRFZ-Si lens	-	-
Formanek [28]	Dipole-type PCA	GaAs	Gold	Aspheric lens	0.80	-
Deva [25]	Conical horn	GaAs	-	Si-lens	-	18.5
Zhu [8]	Bow-tie PCA	LT-GaAs	Ti-Au	No lens	0.18	8.0
	Bow-tie PCA			Si hemispherical lens		11.8
	Bow-tie PCA with lens and combined with metasurface superstrate			FSS		11.9
Malhotra [22]	Dipole planner array	LT-GaAs	Ti-Au	FSS	0.37	13.2

III. ANTENNAS DESIGN PROCEDURE

This section details the design procedure of the realized THz antenna types. The first type of the realized antenna is of a log-spiral type which belongs to the class of frequency-independent antennas [32]. The realized antenna as shown in Fig. 1 schematic is designed to obtain wideband impedance characteristics and good pattern efficiency. In Fig. 1, *r2* describes the outer radius of the antenna which limits the lowest operating frequency of the antenna. The flare rate or the growth rate of the spiral for the increment angle (α) is represented by '*a*', and it controls the wrapping nature of the antenna. Table 2 lists the optimized values of the designed parameter of the proposed antenna of Fig. 1.

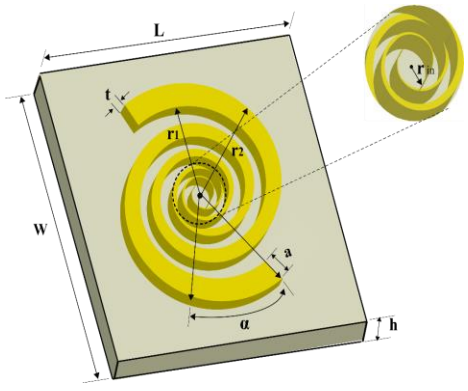

Fig. 1. Schema of the proposed log-spiral THz antenna without lens; *r2*: outer radius of the spiral, *r*: inner radius of the spiral, α: increment angle, *a*: growth rate, *t*: thickness of the conductor (gold) material, *L*: length of the substrate, *W*: width of the substrate, and *h*: thickness of the substrate [6].

Table 2: Log-spiral Antenna design parameters [6]

Parameter	Values(μm)
L (substrate length)	50
W (substrate width)	36
h (substrate thickness)	1
r2 (outer radius of the spiral)	15
r (inner radius of the spiral)	1.03
N (number of turns)	2.5
δ (spiral-patch width)	151
α (increment angle)	12°
a (growth rate)	0.31
t (spiral-patch thickness)	0.05

The Vivaldi antenna structure as shown in Fig. 2 constitutes an exponential curved tapped slot. Besides compact planner structure, the Vivaldi antenna offers additional advantages of the high directive, wider impedance bandwidth, and linear polarization. The exponential tapered profile of the Fig. 2 antenna slot is obtained using the exponential function of (1):

$$f(x) = A\,(e^{ax} - e^{-ax}) + \frac{g}{2}, \tag{1}$$

where

$$A = \frac{\frac{g_2}{2} - \frac{g}{2}}{e^{aL_G} - e^{a}}. \tag{2}$$

In (1), *a* defines curvature coefficient, *g* and g_2 refer to the minimum and maximum width of the tapered slot respectively, and L_G is the length of the antenna patch. Table 2 summarizes the optimized design parameters of the proposed ultra-wideband and high directive Vivaldi antenna for the THz range.

The proposed antenna design of the bowtie THz antenna is shown in Fig. 3. The values of the design parameters of the Fig. 3 antenna are shown in Table 4.

The optimized values of the designed antennas parameters of Tables 2, 3, and 4 are obtained after the detailed conducted parametric study for each antenna type.

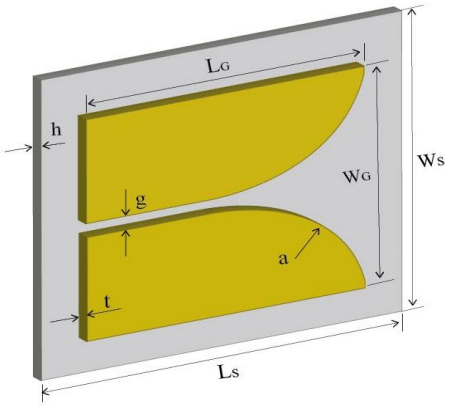

Fig. 2. Schematic of the designed Vivaldi THz antenna without lens: L_S: substrate length, W_S: substrate width, h: substrate thickness, L_G: length of Vivaldi patch, W_G: width of Vivaldi patch, g: minimum width of the tapered slot, a: curvature coefficient, and t: thickness of the Vivaldi patch [7].

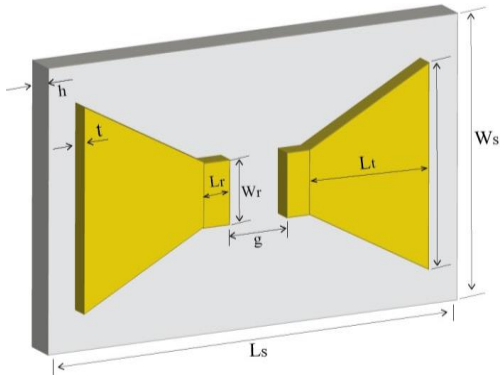

Fig. 3. Schematic of the designed bowtie THz antenna without lens: L_S: substrate length, W_S: substrate width, h: substrate thickness, L_t: length of bowtie patch, g: gap between the bowtie patches, and t: thickness of the bowtie patch [8].

Table 3: Vivaldi Antenna design parameters

Parameter	Values(μm)
L_S (substrate length)	134
W_S (substrate width)	60
h (substrate thickness)	3
L_G (Vivaldi-patch length)	120
W_G (Vivaldi-patch width)	20
g (Minimum width of the tapered slot)	0.1
g_2 (Maximum width of the tapered slot)	22
a (curvature coefficient)	0.7
t (Vivaldi-patch thickness)	0.05

Table 4: Bowtie Antenna design parameters [8]

Parameter	Values(μm)
L_s (substrate length)	347
h (substrate thickness)	2.3
t (bowtie-patch thickness)	0.03
W_s (substrate width)	350
L_t (bowtie-patch length)	117
W_t (bowtie-patch width)	260
W_r (bowtie-port patch length)	13
L_r (bowtie-port patch width)	8
g (gap between the bowtie patches)	3.6

The metal conductor of the designed spiral, Vivaldi, and bowtie antennas has a thickness of 't' and is made of gold conductor (Au) whereas the substrate is made of quartz. The relative permittivity and loss tangent of the used substrate material is 3.78 and 0.0001, respectively. We have used the quartz because of its low-loss characteristics and better capturing of the incident electric fields which is necessary for the high frequencies range operation [33].

The full-wave numerical analysis of the proposed THz antennas is performed in CST MWS for the frequency range of 1 to 6 THz. All antennas are excited using a discrete port in CST MWS. We have used the three-dimensional full-wave electromagnetic field finite integral technique (FIT) available in CST microwave studio-software to precisely calculate. The FIT is a consistent discretization for Maxwell's-equations and it provides a spatial discretization scheme applicable to several electromagnetic problems. The matrix of the discretized fields can be used for efficient simulations. The full-wave numerical simulation of the antennas is performed for the analysis of the antenna's impedance, axial ratio, current distribution, and radiation characteristics.

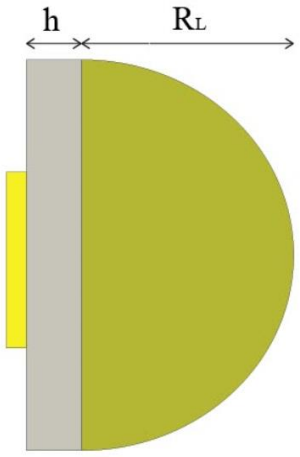

Fig. 4. Schema of the designed spiral THz antenna with hemispherical lens having diameter of R_L [6].

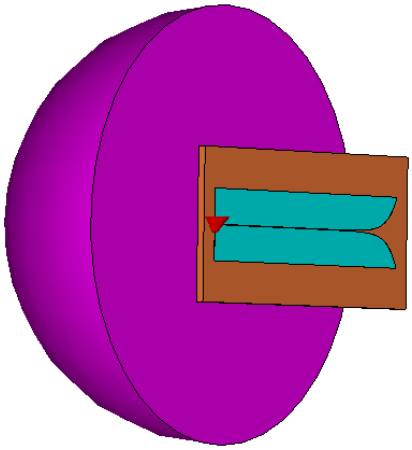

Fig. 5. Schema of the designed Vivaldi THz antenna with hemispherical lens having diameter of R_L [7].

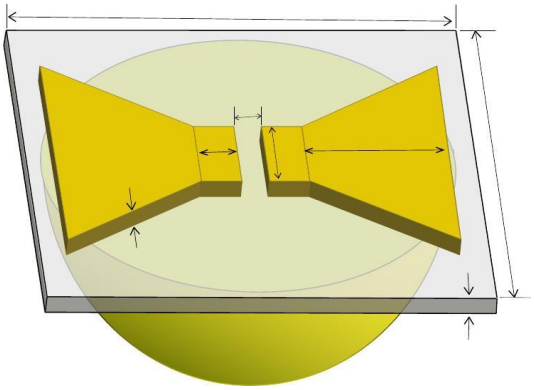

Fig. 6. Schema of the designed bowtie THz antenna with hemispherical lens having diameter of R_L [8].

The analysis of the change in the designed antennas performances is performed by adding hemispherical lenses of silicon on each antenna structure. Figures 4, 5, and 6 depicts the schematics of the antenna structures with the added silicon lens. The diameter (R_L) of the lens is optimized to obtain the wideband impedance, axial ratio bandwidth, and to produce high directivity, gain, and total efficiency of the designed THz antennas. The obtained optimized values of the R_L for spiral, Vivaldi, and bowtie antenna are 140 µm, 85 µm, and 120 µm respectively.

IV. COMPARISON OF DESIGN ANTENNAS WITHOUT LENS

The performance of the designed THz antennas of Figs. 1, 2, and 3 is compared for their -10 dB impedance bandwidth (for $|S_{11}| <$ -10 dB), directivity, maximum directivity, total efficiency, realized gain, total efficiency, and axial ratio characteristics.

Figure 7 shows the comparison of the reflection characteristics of the designed THz antennas. The results show that all three antenna exhibit ultra-wideband impedance matching properties as the $|S_{11}|$ is less than -10 dB for the entire analyzed frequency range of 1 to 6 THz for the spiral and Vivaldi antennas. The -10 dB impedance bandwidth of the realized bowtie antenna is around 2 THz as shown in Fig. 7.

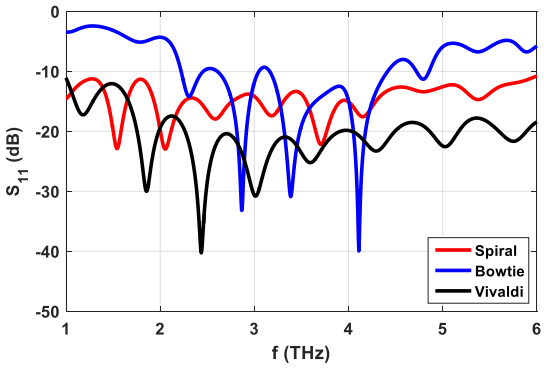

Fig. 7. Comparison of reflection characteristics of the designed THz antennas.

The directivity and maximum directivity results of all three antennas are shown in Figs. 8 and 9 respectively. The comparison reflects that a log-spiral antenna has the best performance as its directivity is higher than the other antenna types as shown in Fig. 8. The results of Fig. 8 reflect that the directivity of all three realized antennas has some variations with the increase in the frequency. The maximum directivity of 10.2 dBi is noted for the Vivaldi antenna as depicted in Fig. 9.

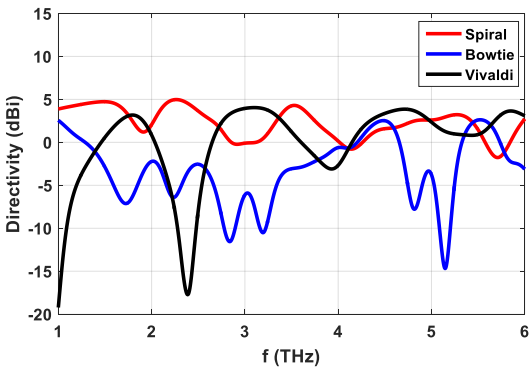

Fig. 8. Comparison of directivity of the designed THz antennas.

Figure 10 shows that the total efficiency of the bowtie antenna is higher than the other two antenna types. The observed total efficiency of the bowtie antenna is higher than 60% in the frequency range of 2.2 THz to 4.9 THz and > 70% efficiency from 2.3 THz to 4.4 THz. The spiral antenna shows good performance with almost flat > 50% total efficiency in the entire analyzed frequency band. The Vivaldi antenna total efficiency is

greater than 10% from 2.2 THz to 6 THz range.

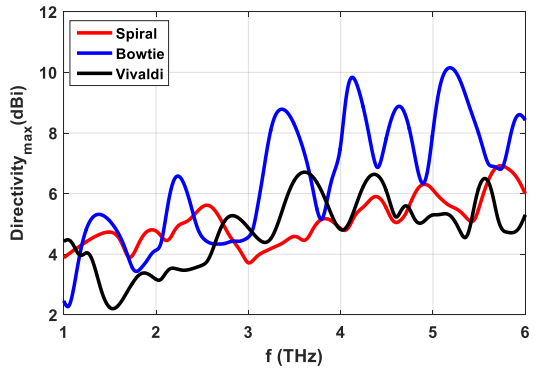

Fig. 9. Comparison of maximum directivity of the designed THz antennas.

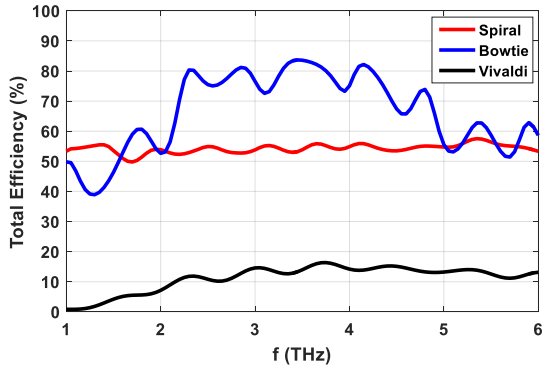

Fig. 10. Comparison of total efficiency of the designed THz antennas.

The difference in the realized gain of the three designed antennas is illustrated in Fig. 11. The realized gain of the spiral antenna is around 0 dBi in the entire frequency range of 1 to 6 THz. The bowtie antenna has realized gain of > -10 dBi in almost whole frequency band of 1 to 6 THz while the Vivaldi antenna shows a similar performance of > -10 dBi realized gain as like bowtie antenna in the frequency range of 2.6 THz to 6 THz. The comparison of results shows that the realized gain of spiral THz antenna is relatively flatter as compared to the other antennas gain characteristics.

Figure 12 reflects the comparison of the axial ratio variations of the spiral, bowtie, and Vivaldi antennas. The AR of the spiral antenna shows that antennas show good circular polarization characteristics from 2 THz to 6 THz frequency range as its AR is less than 3 dB in this frequency band. On the other hand, the other two designed antennas (bowtie and Vivaldi) show very good linear polarization performance with 6 THz AR bandwidth as depicted in Fig. 12. The difference between the AR and impedance bandwidth properties of the spiral antenna could be attributed to the reflections from the end arm of the antenna. The polarizing sense of the reflected waveform is opposite of the outward traveling wave polarization sense and it impacts the lower frequency AR characteristics for the case of the log-spiral antenna as can be noted from the Fig. 12 results.

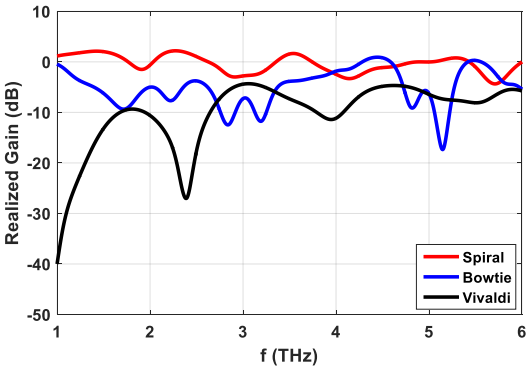

Fig. 11. Comparison of realized gain of the designed THz antennas.

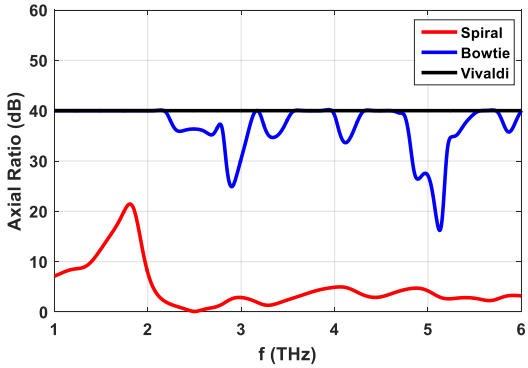

Fig. 12. Comparison of axial ratio of the designed THz antennas.

Figure 13 (a) shows the far-field radiation patterns of the designed spiral antenna at the resonance frequencies of 1.55 THz, 2.05 THz, 3.7 THz, and 5.4 THz respectively. The far-field radiation patterns for the Vivaldi antenna at the resonance frequencies of 1.85 THz, 2.45 THz, 3.6 THz, and 5 THz are shown in Fig. 13 (b). Figure 13 (c) depicts the far-field radiation pattern of the realized bowtie PCA at the resonance frequencies of 2.3 THz, 2.85 THz, 3.35 THz, and 4.1 THz respectively. The spiral and Vivaldi antennas radiation pattern shows an omnidirectional pattern at lower frequencies which changes directional pattern with higher directivity as the frequency increase. The observed gain of the spiral antenna at 1.55 THz and 5.4 THz is 4.68 dBi and 5.11 dBi respectively. The increase in the gain of the Vivaldi antenna from 1.85 THz to 3.6 THz is 3.33 dBi as the observed gain at 1.85 THz and 3.6 THz is 3.38 dBi and 6.71 dBi respectively. As expected, the directional

antenna characteristics for the bowtie antenna can be noted from the directional far-field radiation patterns of the bowtie antenna in Fig. 13 (c). It can be noted that the gain of the bowtie antenna at 2.3 THz and 4.1 THz is 6.33 dBi and 9.8 dBi respectively.

The comparison of Figs. 7-12 results illustrates that all designed antenna shows excellent performance in terms of the impedance and AR bandwidth as compared to all reported antenna structures in [8, 11, 17, 21-25, 28, 29].

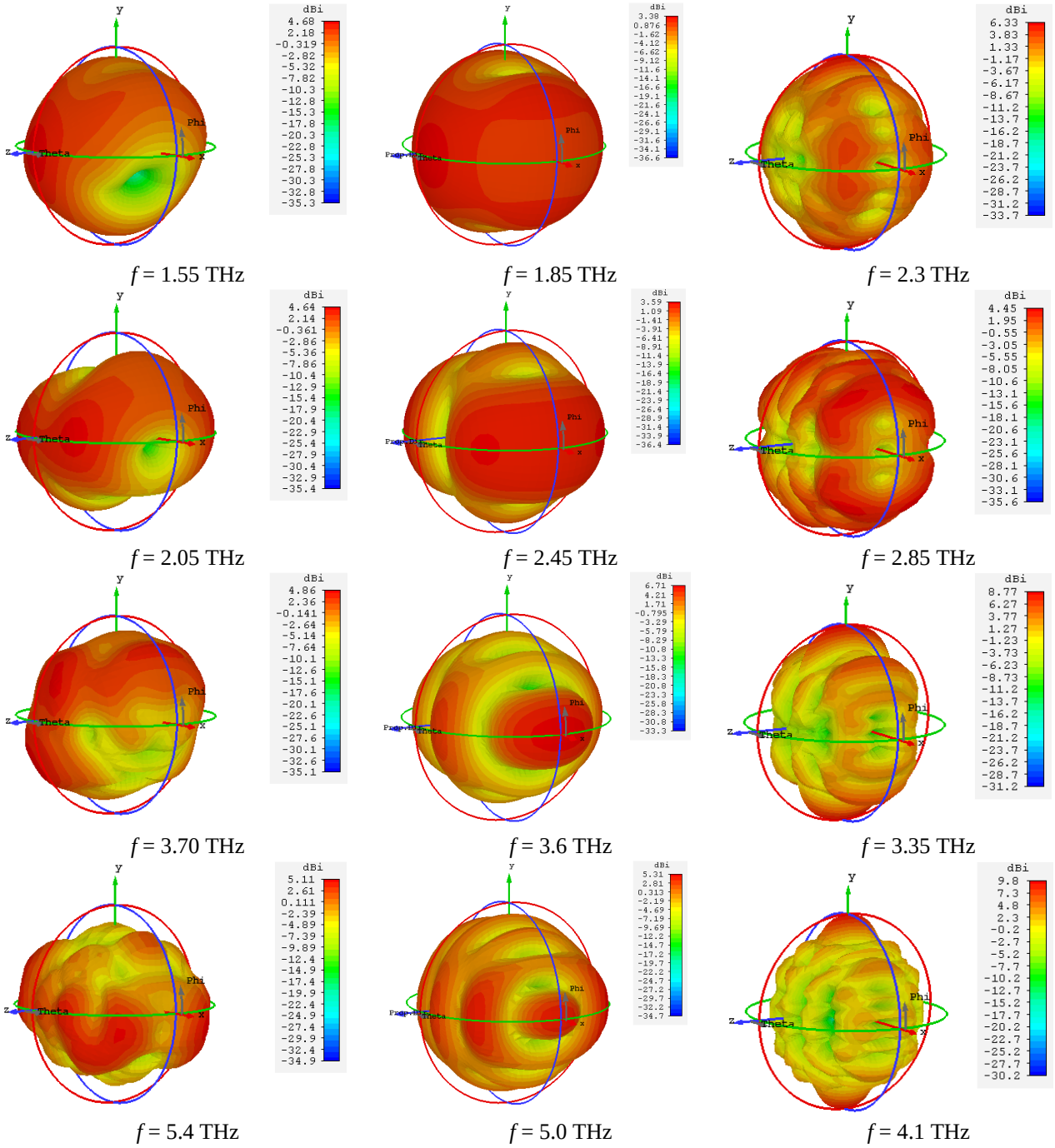

Fig. 13. Comparison of far field radiation patterns of analyzed PCAs without lens.

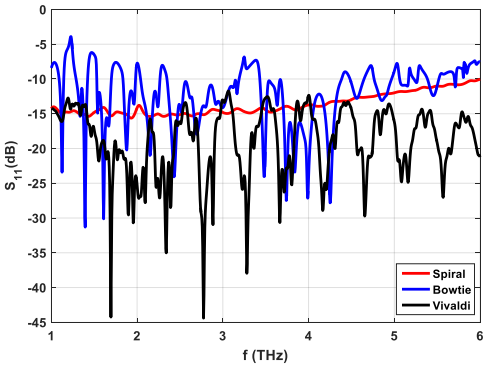

Fig. 14. Comparison of reflection parameter of the designed THz antennas with lens.

V. COMPARISON OF DESIGN ANTENNAS WITH LENS

The performance of the designed spiral, Vivaldi, and bowtie THz antennas is also compared with the integration of the hemispherical lens in the antenna structures. Figures 3-6 depict the structure of antennas with the added lenses.

The comparison of the reflection parameters of the antennas for Figs. 3-6 designs is shown in Fig. 14. It can be noted from Fig. 14 that the addition of the lens in the antenna structure brings a significant change in the resonance characteristics of the antennas. The S_{11} of the spirals antenna becomes flattered with the addition of the lens as compared to the reflection parameter waveform of the same antenna (see Fig. 7). The modification of the bowtie PCA structure for the added lens brings a lot of improvement in its reflection parameters as compared to its characteristics without a lens. The comparison of Figs. 14 and 7 results illustrates that the impedance matching of the designed antenna improves with the addition of the lens in the antenna structure as we are getting lower values of the antenna input reflections. The increase of the intensity of the current distribution around the source point and fewer reflections from the antenna arms results in the better impedance characteristics of the antennas as illustrated in Fig. 14. The results of Fig. 14 deduce that now spiral and Vivaldi antennas exhibit ultra-wideband impedance bandwidth of 6 THz as their reflection properties are less than -10 dB in the analyzed frequency band of 1 to 6 THz.

Figure 15 depicts the comparison of the directive characteristics of the designed antenna with the modified structures of Figs. 3-6. The comparison of Fig. 15 results with Fig. 13 results reflects that the directivity of the antenna has been improved comprehensively in the entire frequency range of 1 to 6 THz. The addition of the lens significantly improves the antenna directivity in the frequency band of 1 to 4 THz as compared to the without lens results of the same antenna in Fig. 8. Around 40-50% increase in the directive of the spiral antenna is observed in the frequency range of the 1 to 5 THz as compared to the without lens directivity results of the same antenna (see Fig. 8). The best improvement is noted for the bowtie antenna with more than 100% improvement in its directivity with the addition of the lens in its structure. The maximum observed directivity of the spiral, Vivaldi, and bowtie antennas is 12 dBi, 10 dBi, and 14 dBi respectively. The radiation performance of the antennas in terms of its total efficiency was also analyzed with the added lenses. The comparison of the total efficiency results of the three analyzed PCAs is depicted in Fig. 16. We note that the total efficiency of the bowtie is highest too for the integrated lens structures of the antennas. The observed total efficiency of the bowtie antenna is more than 60% in the entire band and > 80% in the frequency range of 2 to 5 THz respectively. The average observed total efficiency of the spiral antenna is around 60% from 3 to 6 THz while 50% for the frequency band of 1 to 3 THz. A little decrease in the spiral antenna efficiency is observed in the low-frequency band of 1 to 3 THz as compared to Fig. 10 results of the same antenna without lens structure. The Vivaldi antenna total efficiency performance is much improved as we can observe the average value of around 40% efficiency for this antenna for the frequency range of 2 to 6 THz from Fig. 16 while the around 15% value was noted for the same antenna from Fig. 10 results. The average improvement in the total efficiency of the antennas with the integration of the lens is around 20%, 10%, and 25% for the bowtie, spiral, and Vivaldi antennas as compared to the without lens results of Fig. 10. The improvement of directivity and total efficiency of the antennas with added lens structures is per the improves radiation properties of the antenna as shown in Fig. 14 results.

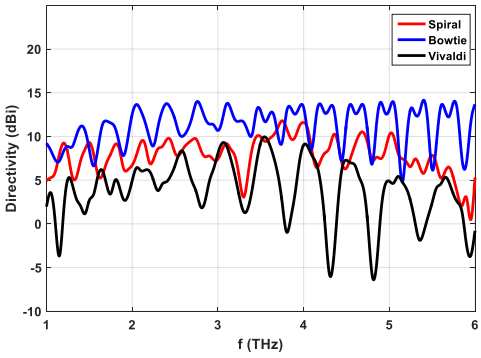

Fig. 15. Comparison of directivity of the designed THz antennas with lens.

The variations in the AR properties of the antennas with added lenses are shown in Fig. 17. The addition of the lens improves the CP characteristics of the spiral antenna in the lower frequency band of 1 to 2 THz while

decorates its performance in a higher frequency region of 5 to 6 THz when compared to the AR characteristics of the same antenna without lens structure in Fig. 12. The AR properties of the Vivaldi antenna remain unchanged while a minor change in the AR variations of the bowtie antenna can be noted as compared to the without lens results of Fig. 12. As like the without lens structure, the performance of the proposed antennas is superior as compared to the legacy designs of [8, 11, 17, 21-25, 28, 29] in terms of -10 dB impedance as well as AR bandwidths.

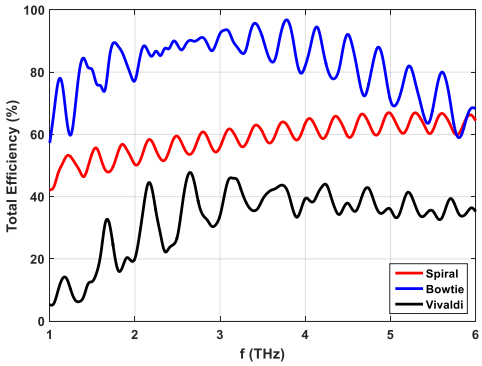

Fig. 16. Comparison of total efficiency of the designed THz antennas with lens.

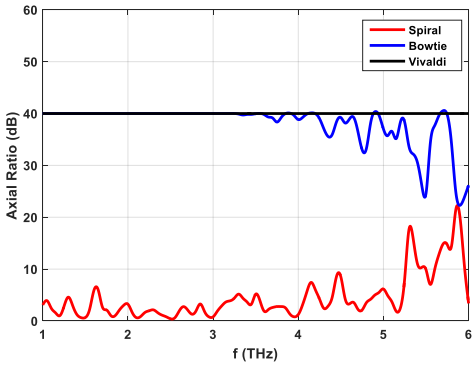

Fig. 17. Comparison of axial ratio of the designed THz antennas with lens.

Figure 18 presents the simulated far-field radiation patterns of the realized PCAs with added lenses in the antenna structures. Figure 18 (a) shows the radiation patterns of the spiral antenna at the resonance frequencies of 1.85 THz, 2.15 THz, 3.45 THz, and 4 THz respectively. It can be noted from Fig. 18 (a) results that the antenna radiation pattern has become directive with the addition of the silicon lens at the backside of the substrate of the designed THz spiral antenna. The observed values of the peak gain at 1.85 THz, 2.15 THz, 3.45 THz, and 4 THz are 9.47 dBi, 10.2 dBi, 10.1 dBi, and 11.3 dBi, respectively. These observed values are greater than the observed gain values from Fig. 13 (a) results.

The simulated far-field radiation pattern at the various resonance frequencies is shown in Fig. 18 (b) for the Vivaldi antenna. The observed values of maximum gain 11.2 dBi @ 1.4 THz, 11.8 dBi @ 2.15 THz, 14.6 dBi @ 4 THz, and 15.3 dBi @ 5.05 THz reflects that the gain of the realized antenna increases with the increase in the operating frequency. These observed gain values are much higher than the recorded gain values for the Vivaldi antenna structure without the lens as depicted in Fig. 13.

The far-field radiations patterns in Fig. 18 (c) for the bowtie antenna reflects that as like the other two antenna types, the gain of the antenna increases due to the directional radiation pattern of the realized antenna structure with the lens. We can note the maximum gain values of 6.75 dBi, 8.39 dBi, 18.6 dBi, and 12.3 dBi for the analyzed resonance frequencies of 1.5 THz, 2.45 THz, 3.05 THz and 4.15 THz respectively for the proposed bowtie antenna.

The comparison of the proposed spiral, Vivaldi, and bowtie antenna structure results with and without lens confirm that the addition of the lens did not only improves the impedance matching and AR properties of the realized antennas but also enhances the directivity of the antennas.

Table 5 summarizes the performance of the proposed antennas in terms of their impedance matching, directivity, and AR bandwidths. The comparison of Tables 1 and 5 results confirms that the proposed antennas impedance, as well as AR bandwidth, is higher than all reported legacy antenna models [8, 11, 17, 21-25, 28, 29] in with/without lens or with frequency selective surfaces.

VI. CONCLUSION

In this study, we reported a detailed comparative study of the performance of the three proposed photoconductive THz antennas. Three different kinds of log spiral, Vivaldi and bowtie PCAs are designed with and without added silicon-based hemispherical lens and their performance in terms of their impedance, as well as AR bandwidth and radiation characteristics (gain, directivity, and efficiency), is compared. The comparison reflects that the designed spiral and Vivaldi PCAs exhibit ultra-wideband impedance bandwidths of 6 THz and bowtie PCA have impedance bandwidth of around 2-3 THz with the added lens in each antenna structure. The bowtie antenna shows superior performance in terms of the high directivity (peak value of 18.2 dBi) and total radiation efficiency (peak value of 95%) as compared to spiral and Vivaldi antennas.

The peak recorded directivity/total radiation efficiencies of the realized spiral and Vivaldi PCAs are 12 dBi/45% and 15 dBi/65%, respectively. The wideband impedance, as well as AR bandwidth and higher radiation characteristics of the proposed THz antennas, makes

them a favorable choice for the wide range of the THz applications (imaging and sensing application, etc.).

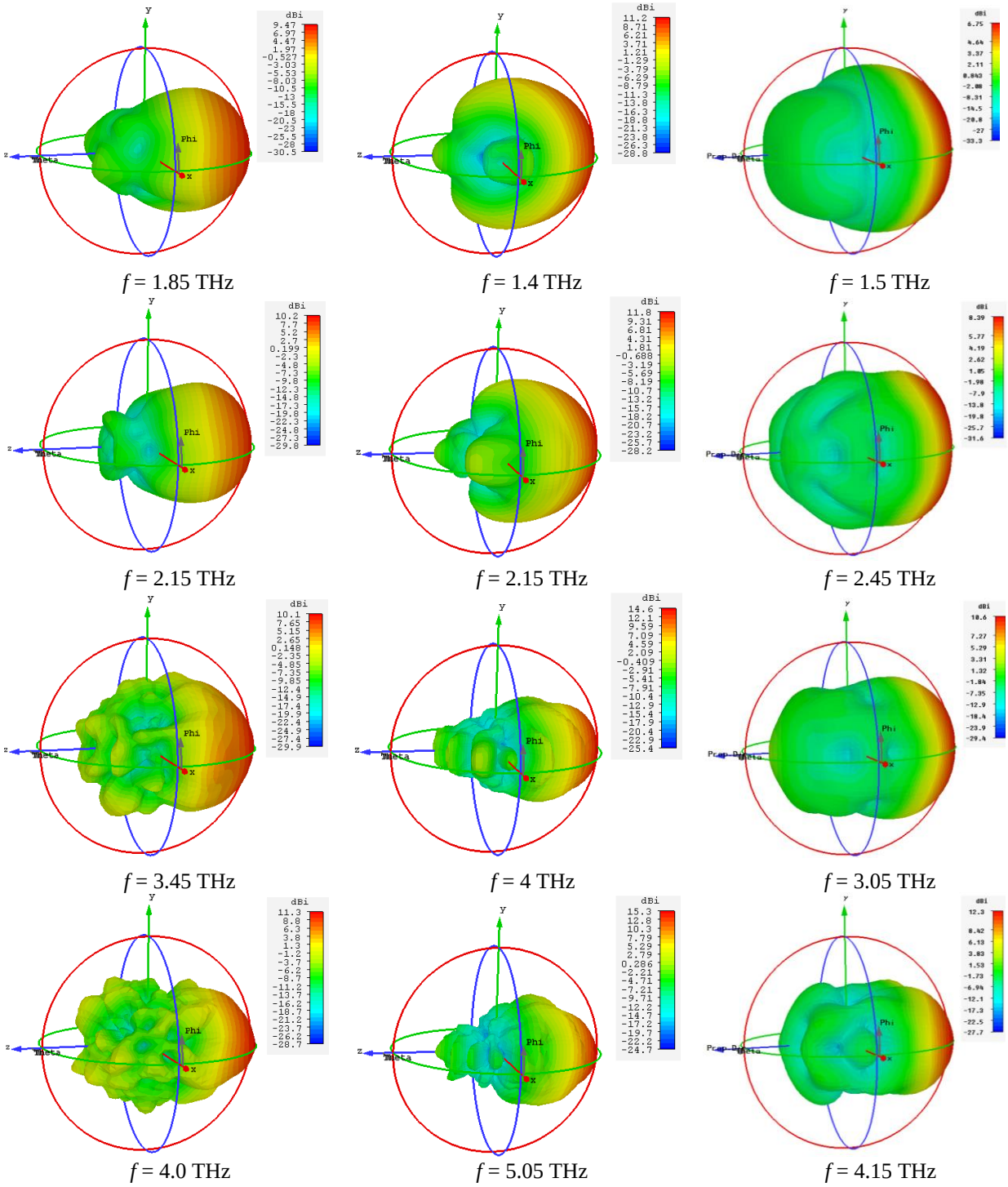

(a) Spiral Antenna (b) Vivaldi Antenna (c) Bowtie Antenna

Fig. 18. Comparison of far-field radiation patterns of designed PCAs with lens for different frequencies.

ACKNOWLEDGMENT

The project was funded by the Deanship of Scientific Research (DSR), King Abdulaziz University, Jeddah, Saudi Arabia under grant no. KEP-Msc-6-135-39. The authors, therefore, acknowledge with thanks DSR technical and financial support.

REFERENCES

[1] P. U. Jepsen, D. G. Cooke, and M. Koch, "Terahertz spectroscopy and imaging – Modern techniques and applications," *Laser & Photonics Reviews*, vol. 5, no. 1, pp. 124-166, Jan. 3, 2011.

[2] I. Kasalynas, R. Venckevicius, and G. Valusis, "Continuous wave spectroscopic terahertz imaging with InGaAs bow-tie diodes at room temperature," *IEEE Sensors Journal*, vol. 13, no. 1, pp. 50-54, 2013.

[3] Y. C. Shen, T. Lo, P. F. Taday, B. E. Cole, W. R. Tribe, and M. C. Kemp, "Detection and identification of explosives using terahertz pulsed spectroscopic imaging," *Applied Physics Letters*, vol. 86, no. 24, p. 241116, June 13, 2005.

[4] M. Bashirpour, M. Forouzmehr, S. E. Hosseininejad, M. Kolahdouz, and M. Neshat, "Improvement of terahertz photoconductive antenna using optical antenna array of ZnO nanorods," *Scientific Reports*, vol. 9, no. 1, p. 1414, Feb. 5, 2019.

[5] I. Malhotra, K. R. Jha, and G. Singh, "Terahertz antenna technology for imaging applications: A technical review," *International Journal of Microwave and Wireless Technologies*, vol. 10, no. 3, pp. 271-290, 2018.

[6] A. Dhiflaoui, A. Yahyaoui, J. Yousaf, T. Aguili, B. Hakim, H. Rmili, and R. Mittra, "Full wave numerical analysis of wideband and high directive log spiral THz photoconductive antenna," *International Journal of Numerical Modelling: Electronic Networks, Devices and Fields*, p. e2761.

[7] J. Yousaf, A. Yahyaoui, B. Hakim, M. Zarouan, W. Zouch, T. Aguili, and H. Rmili, "Design and analysis of ultra-wideband and high directive THz photoconductive Vivaldi antenna," *Applied Computational Electromagnetic Society (ACES) Journal*, vol. 35, no. 10, pp. 1242-1254, Oct. 2020.

[8] N. Zhu and R. W. Ziolkowski, "Photoconductive THz antenna designs with high radiation efficiency, high directivity, and high aperture efficiency," *IEEE Transactions on Terahertz Science and Technology*, vol. 3, no. 6, pp. 721-730, 2013.

[9] A. Dhiflaoui, A. Yahyaoui, J. Yousaf, S. Bashir, B. Hakim, T. Aguili, H. Rmili, and R. Mittra, "Numerical analysis of wideband and high directive bowtie THz photoconductive antenna," *Applied Computational Electromagnetic Society (ACES) Journal*, vol. 35, no. 6, pp. 662-672, June 2020.

[10] N. M. Burford and M. O. El-Shenawee, *Review of Terahertz Photoconductive Antenna Technology* (no. 1 %J Optical Engineering). *SPIE*, 2017, pp. 1-20, 2017.

[11] S.-G. Park, Y. Choi, Y.-J. Oh, and K.-H. Jeong, "Terahertz photoconductive antenna with metal nanoislands," *Optics Express*, vol. 20, no. 23, pp. 25530-25535, Nov. 5, 2012.

[12] L. Hou and W. Shi, "An LT-GaAs terahertz photoconductive antenna with high emission power, low noise, and good stability," *IEEE Transactions on Electron Devices*, vol. 60, no. 5, pp. 1619-1624, 2013.

[13] A. Jooshesh, F. Fesharaki, V. Bahrami-Yekta, M. Mahtab, T. Tiedje, T. E. Darcie, and R. Gordon, "Plasmon-enhanced LT-GaAs/AlAs heterostructure photoconductive antennas for sub-bandgap terahertz generation," *Optics Express*, vol. 25, no. 18, pp. 22140-22148, Sep. 4, 2017.

[14] M. Tani, S. Matsuura, K. Sakai, and S.-I. Nakashima, "Emission characteristics of photoconductive antennas based on low-temperature-grown GaAs and semi-insulating GaAs," *Applied Optics*, vol. 36, no. 30, pp. 7853-7859, Oct. 20, 1997.

[15] M. S. Kong, J. S. Kim, S. P. Han, N. Kim, K. Moon, K. H. Park, and M. Y. Jeon, "Terahertz radiation using log-spiral-based low-temperature-grown InGaAs photoconductive antenna pumped by mode-locked Yb-doped fiber laser," *Optics Express*, vol. 24, no. 7, pp. 7037-7045, Apr. 4, 2016.

[16] S. Yang, M. R. Hashemi, C. W. Berry, and M. Jarrahi, "7.5% optical-to-terahertz conversion efficiency offered by photoconductive emitters with three-dimensional plasmonic contact electrodes," *IEEE Transactions on Terahertz Science and Technology*, vol. 4, no. 5, pp. 575-581, 2014.

[17] A. Gupta, G. Rana, A. Bhattacharya, A. Singh, R. Jain, R. D. Bapat, S. P. Duttagupta, and S. S. Prabhu, "Enhanced optical-to-THz conversion efficiency of photoconductive antenna using dielectric nano-layer encapsulation," *APL Photonics*, vol. 3, no. 5, p. 051706, May 1, 2018.

[18] C. Headley, L. Fu, P. Parkinson, X. Xu, J. Lloyd-Hughes, C. Jagadish, and M. B. Johnston, "Improved performance of GaAs-based terahertz emitters via surface passivation and silicon nitride encapsulation," *IEEE Journal of Selected Topics in Quantum Electronics*, vol. 17, no. 1, pp. 17-21, 2011.

[19] S.-G. Park, K. H. Jin, M. Yi, J. C. Ye, J. Ahn, and K.-H. Jeong, "Enhancement of terahertz pulse emission by optical nanoantenna," *ACS Nano*, vol. 6, no. 3, pp. 2026-2031, Mar. 27, 2012.

[20] M. Bashirpour, S. Ghorbani, M. Forouzmehr, M. R. Kolahdouz, and M. Neshat, "Optical absorption enhancement in LTG-GaAs for efficiency improvement of THz photoconductive antennas," in *2016 Fourth International Conference on Millimeter-Wave and Terahertz Technologies (MMWaTT)*, pp. 14-16, 2016.

[21] A. Jyothi, C. Saha, B. Ghosh, R. Kini, and C. Vaisakh, "Design of a gain enhanced THz bow-tie photoconductive antenna," in *2016 International Symposium on Antennas and Propagation (APSYM)*, pp. 1-3, 2016.

[22] I. Malhotra, K. R. Jha, and G. Singh, "Design of highly directive lens-less photoconductive dipole antenna array with frequency selective surface for terahertz imaging applications," *Optik*, vol. 173, pp. 206-219, Nov. 1, 2018.

[23] K. Han, Y. Park, S. Kim, H. Han, I. Park, and H. Lim, "A terahertz Yagi-Uda antenna for high input impedance," in *2008 33rd International Conference on Infrared, Millimeter and Terahertz Waves*, pp. 1-2, 2008.

[24] R. Singh, C. Rockstuhl, C. Menzel, T. P. Meyrath, M. He, H. Giessen, F. Lederer, and W. Zhang, "Spiral-type terahertz antennas and the manifestation of the Mushiake principle," *Optics Express*, vol. 17, no. 12, pp. 9971-9980, June 8, 2009.

[25] U. Deva and C. Saha, "Gain enhancement of photo-conductive THz antenna using conical GaAs horn and Si lens," in *2016 International Symposium on Antennas and Propagation (APSYM)*, pp. 1-3, 2016.

[26] G. Matthäus, S. Nolte, R. Hohmuth, M. Voitsch, W. Richter, B. Pradarutti, S. Riehemann, G. Notni, and A. Tünnermann, "Large-area microlens emitters for powerful THz emission," *Applied Physics B*, vol. 96, no. 2, pp. 233-235, Aug. 1, 2009.

[27] A. Singh and S. S. Prabhu, "Microlensless interdigitated photoconductive terahertz emitters," *Optics Express*, vol. 23, no. 2, pp. 1529-1535, Jan. 26, 2015.

[28] F. Formanek, M.-A. Brun, T. Umetsu, S. Omori, and A. Yasuda, "Aspheric silicon lenses for terahertz photoconductive antennas," *Applied Physics Letters*, vol. 94, no. 2, p. 021113, Jan. 12, 2009.

[29] Q. Yu, J. Gu, Q. Yang, Y. Zhang, Y. Li, Z. Tian, C. Ouyang, J. Han, J. F. O. Hara, and W. Zhang, "All-dielectric meta-lens designed for photo-conductive terahertz antennas," *IEEE Photonics Journal*, vol. 9, no. 4, pp. 1-9, 2017.

[30] B. Pradarutti, R. Müller, W. Freese, G. Matthäus, S. Riehemann, G. Notni, S. Nolte, and A. Tünnermann, "Terahertz line detection by a microlens array coupled photoconductive antenna array," *Optics Express*, vol. 16, no. 22, pp. 18443-18450, Oct. 27, 2008.

[31] R. Mendis, C. Sydlo, J. Sigmund, M. Feiginov, P. Meissner, and H. L. Hartnagel, "Spectral characterization of broadband THz antennas by photoconductive mixing: toward optimal antenna design," *IEEE Antennas and Wireless Propagation Letters*, vol. 4, pp. 85-88, 2005.

[32] V. Rumsey, "Frequency independent antennas," in *1958 IRE International Convention Record, IEEE*, vol. 5, pp. 114-118, 1966.

[33] W. Amara, A. Alghamdi, D. Oueslati, N. Eltresy, M. Sheikh, H. Rmili, "Analysis of infrared nano-antennas material properties for solar energy collection," *Applied Computational Electromagnetic Society (ACES) Journal*, vol. 35, no. 3, pp. 258-266, Mar. 2020.